
LoRIF: Low-Rank Influence Functions for Scalable Training Data Attribution

Shuangqi Li¹ Hieu Le² Jingyi Xu³ Mathieu Salzmann¹

Abstract

Training data attribution (TDA) identifies which training examples most influenced a model’s prediction. The best-performing TDA methods exploits gradients to define an influence function. To overcome the scalability challenge arising from gradient computation, the most popular strategy is random projection (e.g., TRAK, LoGRA). However, this still faces two bottlenecks when scaling to large training sets and high-quality attribution: (i) storing and loading projected per-example gradients for all N training examples, where query latency is dominated by I/O; and (ii) forming the $D \times D$ inverse Hessian approximation, which costs $O(D^2)$ memory. Both bottlenecks scale with the projection dimension D , yet increasing D is necessary for attribution quality—creating a quality–scalability tradeoff. We introduce **LoRIF (Low-Rank Influence Functions)**, which exploits low-rank structures of gradient to address both bottlenecks. First, we store rank- c factors of the projected per-example gradients rather than full matrices, reducing storage and query-time I/O from $O(D)$ to $O(c\sqrt{D})$ per layer per sample. Second, we use truncated SVD with the Woodbury identity to approximate the Hessian term in an r -dimensional subspace, reducing memory from $O(D^2)$ to $O(Dr)$. On models from 0.1B to 70B parameters trained on datasets with millions of examples, LoRIF achieves up to 20 \times storage reduction and query-time speedup compared to LoGRA, while matching or exceeding its attribution quality. LoRIF makes gradient-based TDA practical at frontier scale.

1. Introduction

Training data attribution (TDA) answers a fundamental question: which training examples were most responsible for a given model’s prediction on a test input? This capability enables diverse applications such as debugging incorrect predictions by tracing them to mislabeled or anomalous training data, detecting data poisoning attacks, curating high-quality training sets, and understanding how models generalize (Koh & Liang, 2017; Ilyas et al., 2022). As models grow larger and are trained on increasing web-scale datasets, the need for reliable, scalable attribution methods becomes more pressing.

Influence functions (Koh & Liang, 2017) provide a theoretically-grounded approach to TDA: they approximate leave-one-out retraining via the use of gradients and the inverse Hessian. However, all existing methods for computing influence functions are expensive—iterative solvers require repeated Hessian–vector products across the training set, while simpler similarity methods sacrifice attribution accuracy for speed (Section 2.2). Modern variants—TRAK (Park et al., 2023), LoGRA (Choe et al., 2024), and TrackStar (Chang et al., 2024)—improve scalability by storing projected per-example gradients and using a damped Gauss–Newton Hessian approximation. However, while these projection-based methods represent the current scalability frontier for gradient-based TDA, they still face fundamental bottlenecks at scale.

Specifically, the bottlenecks of projection-based TDA methods are twofold. First, **gradient storage and I/O**: storing projected per-example gradients for all N training examples requires $O(ND)$ space, where D is the effective projection dimension (the total dimension of the stored gradient per example); at query time, loading these gradients dominates latency (around 96% of the query time). Second, **inverse Hessian scaling**: forming and storing the $D \times D$ inverse Hessian approximation costs $O(D^2)$ memory. Both bottlenecks scale with D —yet increasing D is key to high attribution quality. This creates a quality–scalability tradeoff: accurate attribution (large D) is impractical, while tractable attribution (small D) degrades quality.

Here, we introduce LoRIF, which breaks this tradeoff by

¹EPFL, Switzerland ²UNC Charlotte, USA ³Stony Brook University, USA. Correspondence to: Mathieu Salzmann <mathieu.salzmann@epfl.ch>, Shuangqi Li <shuangqi.li@epfl.ch>.

Table 1. Different families of TDA methods. The attribution quality of projection-based influence functions is heavily dependent on the projection dimension D , as shown in Figure 1. Projection-based methods represent the current scalability frontier, and LoRIF pushes this frontier further.

Method Family	Scalability	Accuracy	Main bottleneck(s)
Simulation-based methods	Very poor	Good	Many counterfactual training runs
Trajectory-aware methods	Poor	Good	Computing through the training trajectory/checkpoints
Infl. functions (parameter-space)	Poor	Fair	Recomputing high-dimensional per-example gradients
Infl. functions (projection-based)	Fair	Fair	Storing and loading projected gradients; forming H^{-1}
Grad./Repr. similarity	Fair	Poor	Storing and loading/Limited attribution faithfulness
LoRIF (ours)	Good	Fair	—

exploiting a key property: **neural-network gradients have low effective rank** (see Section 2.3), both within layers (per-example) and in the aggregate across examples. To address the storage and I/O bottleneck, we therefore store each projected per-example gradient as a rank- c factorization, reducing storage and query-time I/O from $O(D)$ to $O(c\sqrt{D})$ per layer. To address the $D \times D$ memory bottleneck, we compute a truncated SVD of the gradient matrix and exploit the Woodbury identity to compute the curvature term in an r -dimensional subspace without forming a dense $D \times D$ inverse—reducing memory cost from $O(D^2)$ to $O(Dr)$. Together, these approximations enable increasing D (improving quality) while keeping both storage/I/O and curvature costs tractable.

We evaluate LoRIF on language models spanning three orders of magnitude: GPT2-small (124M parameters, 233k training examples), Olmo3-7B (7B parameters, 2.2M training examples), and Apertus-70B (70B parameters, 3.8M training examples). Compared to the state-of-the-art LoGRA, LoRIF yields

- **Storage:** 2.3 ~ 20 times reduction,
- **Query-time speedup:** 1.3 ~ 20 times faster influence computation,
- **Quality:** matching or exceeding LDS and Tail-patch scores.

In other words, LoRIF makes gradient-based TDA practical at frontier scale without sacrificing attribution quality. To our knowledge, this is the first time that gradient-based TDA is practical at this scale, without the need to recompute per-example gradients for each query batch.

2. Background and Related Work

2.1. Influence Functions

A theoretically-grounded way to estimate the impact of a training sample on a model’s prediction consists of defining an influence function based on the model’s gradients. Be-

low, we provide some background on this approach, before delving into the attempts that have been made to improve the scalability of this strategy.

Classical influence functions. Given a model with parameters θ^* trained to minimize an empirical risk, the influence of a training sample x_{tr} on a test sample x_{te} can be approximated as (Koh & Liang, 2017)

$$\mathcal{I}(x_{tr}, x_{te}) = g_{te}^\top H^{-1} g_{tr}, \quad (1)$$

where g_{tr} and g_{te} are the gradients of the loss with respect to the model parameters on the training and test samples, and H is the Hessian of the training loss. This formulation approximates how the model’s prediction on the test sample x_{te} would change if the training sample x_{tr} were infinitesimally upweighted.

Gauss-Newton Hessian approximation. For deep models, the Hessian matrix H is very large and typically positive *semi*-definite, making it intractable to compute and invert. As such, recent works have approximated the Hessian using the damped Gauss-Newton matrix (Teso et al., 2021; Bae et al., 2022; Grosse et al., 2023; Choe et al., 2024; Chang et al., 2024)

$$H \approx G^\top G + \lambda I, \quad (2)$$

where $G \in \mathbb{R}^{N \times D}$ is the matrix of gradients (or projected gradients, as discussed below) for all N training samples, and $\lambda > 0$ is a damping term. With this approximation, the influence function in Equation (1) becomes:

$$\mathcal{I}(x_{tr}, x_{te}) \approx g_{te}^\top (G^\top G + \lambda I)^{-1} g_{tr}. \quad (3)$$

However, calculating Eq. (2) in the original parameter space is often intractable, as the gradient can have billions of dimensions.

Inverse Hessian-vector product. Instead of explicitly forming the Hessian or its approximation, one can directly approximate the inverse Hessian-vector products

(iHVP). Early iHVP approximations include stochastic Neumann-series estimators such as LiSSA (Agarwal et al., 2017) and Krylov-subspace methods such as Arnoldi iteration (Schioppa et al., 2022). Grosse et al. (2023) proposes using (E)K-FAC for iHVP approximation, leveraging the Kronecker structure of gradient matrices. ASTRA (Wang et al., 2025a) further reduces the iterations needed for accurate iHVP estimation by using EKFAC as a preconditioner for iterative Neumann-series updates. In large-scale retrieval regimes, however, a dominant bottleneck of these methods that work in the *original parameter space* is often the need to re-compute per-example gradients for a massive training set.

Random projection for tractability. Even with the Gauss-Newton Hessian and iHVP approximations, working in the original parameter space is a computational and storage bottleneck at scale, requiring storing or recomputing high-dimensional per-example gradients. Wojnowicz et al. (2016) and Park et al. (2023) project the (flattened) gradients to a lower-dimensional space using random projection matrices, making Eq. (2) tractable. LoGRA (Choe et al., 2024) and TrackStar (Chang et al., 2024) reduce the memory cost of random projection matrices by applying *two-sided* random projections: for each linear layer with input dimension I and output dimension O , the gradients are projected from $\mathbb{R}^{O \times I}$ to $\mathbb{R}^{d_2 \times d_1}$ using separate random matrices $P_{in} \in \mathbb{R}^{I \times d_1}$ and $P_{out} \in \mathbb{R}^{O \times d_2}$. For an *effective projection dimension* $D = d_1 \cdot d_2$, the memory cost of the random projection matrices for each layer is reduced from $O(DIO)$ to $O(d_1I + d_2O)$.

2.2. Other TDA Families

Training data attribution methods span a wide spectrum of scalability and quality tradeoffs. We survey the major families to contextualize LoRIF and justify our choice to build on influence functions. Table 1 summarizes the tradeoffs.

Similarity-based methods. TracIn (Pruthi et al., 2020) estimates influence by aggregating gradient dot products across training checkpoints, avoiding Hessian inversion but requiring multiple checkpoints and repeated gradient evaluations. A common lightweight variant uses only the final checkpoint, reducing to gradient-similarity scoring (Charpiat et al., 2019), which is more efficient but can be less faithful than curvature-aware influence estimators. Representer point selection (Yeh et al., 2018) instead uses representations for similarity scoring, with weights derived from the last-layer gradients. Hanawa et al. (2020) directly compare representations and avoid gradient computation. These methods typically scale better than influence-style methods but provide weaker attribution accuracy.

Trajectory-aware methods. Unrolling/hypergradient methods estimate attribution by differentiating through the training trajectory, avoiding the local-optimality assumptions underlying classical influence functions. Canonical examples include SGD-Influence (Hara et al., 2019) and HyDRA (Chen et al., 2021), which estimate counterfactual effects by differentiating through (parts of) the training trajectory, improving faithfulness but incurring costs that grow with the number of steps/checkpoints. SOURCE (Bae et al., 2024) bridges influence function and unrolling, reducing overhead by segmenting the training trajectory. Overall, these methods trade scalability for fidelity.

Simulation-based methods. Simulation-based methods estimate influence via many counterfactual training runs on perturbed datasets. Data Shapley (Ghorbani & Zou, 2019) approximates Shapley values via Monte Carlo permutations. Datamodeling (Ilyas et al., 2022) fits a predictor of the model behavior across many subset-trained models. Simfluence (Guu et al., 2023) learns a simulator of loss trajectories under hypothetical training curricula. Despite high fidelity, the need for many extra runs makes these methods impractical at large scale.

2.3. Low-Rank Gradients in Neural Networks

LoRIF exploits two complementary low-rank phenomena observed in neural-network gradients:

Per-example gradients have low effective rank. In practice, it has been shown that the weight gradients of a linear layer are often well approximated by low-rank matrices, a phenomenon leveraged by gradient compression methods (Wang et al., 2018; Vogels et al., 2019; 2020) and memory-efficient training (Zhao et al., 2024; Gooneratne et al., 2020; Liang et al., 2024). A related concept is Low-Rank Adaptation (LoRA) (Hu et al., 2022; Hao et al., 2024; Liu et al., 2024), which enables parameter-efficient fine-tuning by constraining the weight updates to low-rank subspaces.

Cross-example gradients have low effective rank. Empirical studies of deep-network Hessians frequently report a *spiked* spectrum: a small number of dominant directions together with a large bulk of near-zero eigenvalues (Sagun et al., 2016; Wu et al., 2020). Related work reports similar spectral concentration for Fisher/Fisher-variant curvature (Karakida et al., 2019; Singh et al., 2021). Together, these findings suggest that the gradient Gram matrix $G^\top G$, as well as G itself, can have low *effective rank* in practice.

Here, we exploit these observations to develop a TDA method that scales to models with billions of parameters without sacrificing attribution quality.

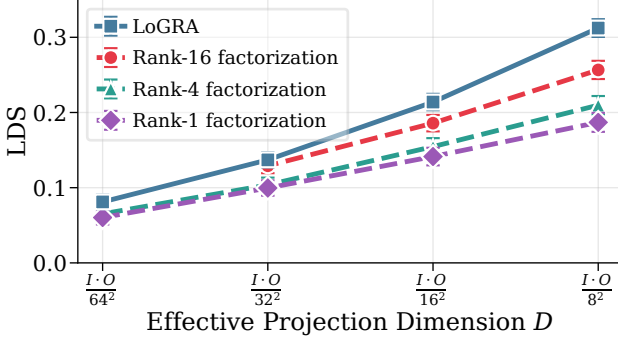


Figure 1. Attribution quality (LDS) vs. effective projection dimension D . We compare LoGRA (no factorization) against rank- c factorization for $c \in \{1, 4, 16\}$ on GPT2-small, varying D by setting $d_1 = \frac{I}{f}$ and $d_2 = \frac{O}{f}$ for $f \in \{64, 32, 16, 8\}$ (so $D = \frac{I \cdot O}{f^2}$).

3. Method: LoRIF

LoRIF follows the standard TRAK/LoGRA pipeline but addresses the two scalability bottlenecks: (1) gradient storage and query-time I/O, and (2) inverse Hessian scaling. Our method follows three steps: first, we compute and store per-example gradients using low-rank factorization (§3.1); second, we compute an inverse Hessian approximation via truncated SVD and the Woodbury identity (§3.2); third, we compute influence scores at query time using the stored low-rank factors and the truncated inverse Hessian (§3.3).

3.1. Per-Example Gradients

Consider a model with L linear layers. Layer ℓ has input dimension I_ℓ , output dimension O_ℓ , and weight matrix $W_\ell \in \mathbb{R}^{O_\ell \times I_\ell}$. Following LoGRA, we apply two-sided random projections with matrices $P_{in}^\ell \in \mathbb{R}^{I_\ell \times d_1^\ell}$ and $P_{out}^\ell \in \mathbb{R}^{O_\ell \times d_2^\ell}$. For training sample i at layer ℓ , let $X_i^\ell \in \mathbb{R}^{T \times I_\ell}$ be the input activations and $\delta Y_i^\ell \in \mathbb{R}^{T \times O_\ell}$ the output gradients across T tokens. The projected gradient matrix is then

$$\tilde{G}_i^\ell = (X_i^\ell P_{in}^\ell)^\top (\delta Y_i^\ell P_{out}^\ell) \in \mathbb{R}^{d_1^\ell \times d_2^\ell}. \quad (4)$$

We define the *effective projection dimension* for layer ℓ as $D_\ell = d_1^\ell \cdot d_2^\ell$, and the flattened per-example gradient vector $g_i^\ell := \text{vec}(\tilde{G}_i^\ell) \in \mathbb{R}^{D_\ell}$. We then denote by $G^\ell \in \mathbb{R}^{N \times D_\ell}$ the matrix whose i -th row is $(g_i^\ell)^\top$. In what follows, we omit the layer index ℓ when the context is clear.

Rather than storing \tilde{G}_i^ℓ directly, we store a rank- c factorization

$$\tilde{G}_i^\ell \approx u_i^\ell (v_i^\ell)^\top, \quad u_i^\ell \in \mathbb{R}^{d_1^\ell \times c}, \quad v_i^\ell \in \mathbb{R}^{d_2^\ell \times c}, \quad (5)$$

computed via a few block power iterations. This reduces storage per layer per sample from $d_1^\ell d_2^\ell$ floats to $c(d_1^\ell + d_2^\ell)$ floats.

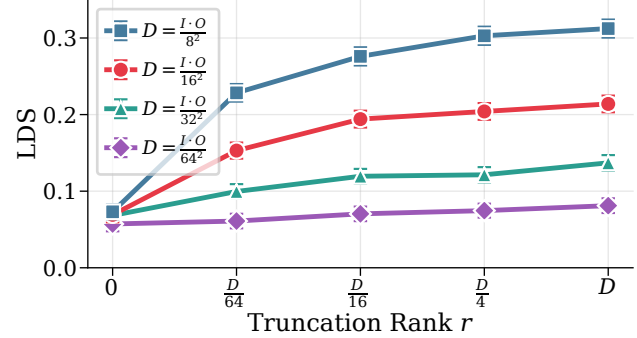


Figure 2. Attribution quality (LDS) vs. truncation rank r for the low-rank inverse Hessian approximation, shown for varying effective layer dimensions D . Rank factorization is **not** used. $r = 0$ corresponds to discarding the curvature information and degrading to naive dot product. We use GPT2-small and train it on WikiText-103, with the number of training examples $N \gg D$.

Figure 1 validates this approximation and guides our choice of c . Even the most aggressive compression ($c = 1$) yields meaningful attribution quality. Moreover, for a fixed storage budget, increasing D improves quality more than increasing c : quadrupling D (which doubles storage for the low-rank factorization) yields larger gains than quadrupling c at fixed D (which quadruples storage). This indicates that $c = 1$ should be used for the best cost efficiency, prioritizing larger D over a higher factorization rank.

Grosse et al. (2023) also leverage the low-rank structure of gradients, but for a different purpose: they store 32-rank approximations of preconditioned *query* gradients in order to fit more of them in memory and amortize the cost of re-computing training gradients. We instead factorize *training* gradients with lower ranks, prioritizing storage reduction of the N -example database over per-gradient fidelity.

3.2. Inverse Hessian Approximation

To efficiently compute Eq. (3), projection-based methods explicitly form and store $K = (G^\top G + \lambda I)^{-1} \in \mathbb{R}^{D \times D}$ in the projected space, avoiding slower iterative iHVP solvers and gradient recomputation. However, forming this matrix costs $O(D^3)$ time and $O(D^2)$ space, which becomes infeasible as D grows. Following Choe et al. (2024); Chang et al. (2024), we form K individually for each layer (a block-diagonal Hessian approximation), but this alone still limits D_ℓ to roughly 10^5 in practice.

This constraint conflicts with the quality gains from larger D . As Figure 1 shows, attribution quality improves substantially as D increases, suggesting continued gains beyond the feasible range. For example, setting $d_1 = I/4$ and $d_2 = O/4$ yields $D = IO/16$, which can exceed 1.5×10^5 for some layers in GPT2-small. Since $H \in \mathbb{R}^{D \times D}$, storing H or H^{-1} alone requires more than 80GB in FP32,

and even more for computing the inverse. To unlock these gains, we need an inverse Hessian approximation that scales sublinearly in D .

To further reduce the cost of forming and storing $(G^\top G + \lambda I)^{-1}$, we leverage a rank- r truncated SVD of $G \in \mathbb{R}^{N \times D}$ (layer index ℓ omitted for brevity), i.e.,

$$G \approx U_r \Sigma_r V_r^\top, \quad (6)$$

$$U_r \in \mathbb{R}^{N \times r}, \Sigma_r \in \mathbb{R}^{r \times r}, V_r \in \mathbb{R}^{D \times r}.$$

with $r \ll \min(N, D)$. We perform randomized SVD (Halko et al., 2011) once after collecting all training gradients, reconstructing rows of G batch-by-batch from the stored low-rank factors without materializing G in memory.

The low-rank Hessian approximation is then $H \approx V_r \Sigma_r^2 V_r^\top + \lambda I$. Applying the Woodbury identity gives

$$(V_r \Sigma_r^2 V_r^\top + \lambda I)^{-1} = \frac{1}{\lambda} I - \frac{1}{\lambda^2} V_r \underbrace{\left(\Sigma_r^{-2} + \frac{1}{\lambda} I_r \right)^{-1}}_{r \times r \text{ diagonal}} V_r^\top. \quad (7)$$

This reduces the time complexity of approximating H^{-1} from $O(ND^2 + D^3)$ to $O(NDc + NDr)$ and the space complexity from $O(D^2)$ to $O(Dr)$. We store only $V_r \in \mathbb{R}^{D \times r}$ and $\Sigma_r \in \mathbb{R}^r$ —reducing the memory cost of storing the H^{-1} approximation from $O(D^2)$ to $O(Dr)$.

We evaluate the quality-efficiency tradeoff of this approximation by varying r and D . In particular, Figure 2 reports attribution quality (LDS) as a function of r for different effective dimensions D , compared against the full-rank baseline from Eq. (3). These results confirms that attribution quality approaches the full-rank level for $r \ll D$. Additional evidence and analysis of the spectrum concentration of G are provided in Appendix C.

3.3. Influence Scores

For a given query example x_{te} , we denote the corresponding flattened projected gradient as g_{te} . Similarly, we use x_{tr} and g_{tr} to denote any example in the training set and its corresponding flattened projected gradient.

At query time, we load the stored Σ_r , V_r (Eq. (6)) and form g_{te} from the stored low-rank factors from Eq. (5) in GPU memory. For the training gradients g_{tr} , we load their low-rank factors from high-performance storage (e.g., NVMe) to GPU memory batch-by-batch to form them on the fly during the influence computation. We project the gradients into the r -dimensional subspace as

$$g'_{tr} = V_r^\top g_{tr} \in \mathbb{R}^r, \quad g'_{te} = V_r^\top g_{te} \in \mathbb{R}^r. \quad (8)$$

Substituting Eq. (6) and Eq. (7) into Eq. (3), the influence

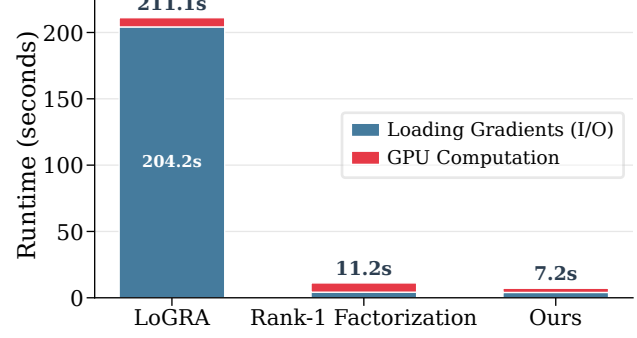


Figure 3. Time spent in loading gradients and GPU computation. We visualize the query-time latency breakdown for different methods, with the same effective projection dimension $D = \frac{I \cdot O}{8^2}$ and a truncation rank $r = \frac{D}{16}$ for each layer of GPT2-small. “Ours” means combining rank-1 factorization and the truncated SVD approximation.

becomes

$$\mathcal{I}(x_{tr}, x_{te}) \approx \frac{1}{\lambda} g_{te}^\top g_{tr} - \frac{1}{\lambda^2} (g'_{te})^\top \left(\Sigma_r^{-2} + \frac{1}{\lambda} I_r \right)^{-1} g'_{tr}. \quad (9)$$

The first dot product $g_{te}^\top g_{tr} = \langle \tilde{G}_{te}, \tilde{G}_{tr} \rangle_F$ can be computed directly from the rank- c factors as $(u_{te}^\top u_{tr})(v_{te}^\top v_{tr})$, costing $O(c^2(d_1 + d_2))$ instead of $O(d_1 d_2)$. The second term costs $O(r)$ since the middle matrix is diagonal.

Let us Consider scoring N_q query examples against all N training examples. LoRIF achieves speedup from:

- **Reduced I/O.** LoRIF loads $c(d_1 + d_2)$ floats per training sample per layer instead of $d_1 d_2$ —a compression ratio of $d_1 d_2 / c(d_1 + d_2) \approx \min(d_1, d_2) / 2$.
- **Reduced computation.** LoGRA requires $O(D^2 N_q)$ for applying H^{-1} to query gradients, plus $O(D N N_q)$ for pairwise dot products. LoRIF requires $O(r D (N + N_q))$ to project all gradients via V_r , plus $O(c^2(d_1 + d_2) N N_q + r N N_q)$ for influence computation via Eq. (9). When $N_q \ll N$ and r is relatively small (e.g., $r \approx N_q$), the projection cost $O(r D (N + N_q))$ is comparable to LoGRA’s scoring cost $O(D N N_q)$. Further, when c is small (e.g., $c = 1$), the per-pair cost drops substantially from $O(D)$ to $O(c^2(d_1 + d_2) + r)$. Most of our experiments in Section 4 fall into this case.

Figure 3 confirms this analysis with $N = 233k$, $N_q = 1k$, $D/r = 16$, and D being up to 37k for some layers. LoGRA is I/O-bounded (96% of 211s spent loading gradients). Rank-1 factorization alone reduces I/O by $\sim 40\times$, cutting the total time to 11s. Adding the truncated SVD approximation further reduces computation, yielding 7s in total—a $30\times$ speedup over LoGRA.

We acknowledge that both the rank-1 factorization and the truncated SVD introduce approximation errors. However,

as we will show in Section 4, LoRIF enables recovering or exceeding LoGRA’s attribution quality while enjoying the efficiency gains because we can increase D beyond the feasible range of LoGRA.

4. Experiments

We evaluate LoRIF on three axes: (1) storage reduction, (2) query-time speedup, and (3) attribution quality compared to baseline methods. We describe our choices for baselines, metrics, models, and datasets in the following subsection.

4.1. Experimental Setup

Baseline Methods. We select the following baseline methods from different TDA families for a comprehensive evaluation.¹

- **LoGRA** (Choe et al., 2024): A projection-based method that stores the projected per-example gradients and uses a damped Gauss-Newton Hessian approximation. Compared to TRAK (Park et al., 2023), LoGRA is more scalable as it leverages two-sided random projections.²
- **EK-FAC** (Grosse et al., 2023): A parameter-space method that leverages the eigenvalue-corrected K-FAC Hessian approximation for faster iHVP computation, requiring recomputation of training gradients for each query batch.
- **GradDot** (Charpiat et al., 2019; Pruthi et al., 2020): A simple gradient-based method that uses a dot product between the query and training gradients to approximate the influence. Two-sided random projections are applied to the gradients.
- **RepSim** (Hanawa et al., 2020): A simple method that computes the cosine similarity between the representation of the query and the training examples. We use the hidden states of the last token in the last layer of the model as the representation.

Metrics. We select the following metrics for assessing the attribution quality and efficiency.

- **LDS (Linear Datamodeling Score)** (Park et al., 2023): Measures how well the predicted influence scores linearly predict changes in model output when the training data is subsampled. LDS is the gold-standard metric but requires hundreds of retraining runs, making it feasible only for smaller-scale experiments.
- **Tail-patch score** (Chang et al., 2024): A scalable metric measuring the direct contribution of the retrieved training

¹We do not include the unrolling-based method SOURCE (Bae et al., 2024) in our evaluation because it lacks a public implementation.

²TrackStar (Chang et al., 2024) is similar to LoGRA, but is not included in our evaluation because its innovations aim to improve fact tracing tasks specifically.

examples. For each query, we identify the top- k training proponents, perform one incremental training step (a “tail patch”) on the final checkpoint using this batch, and measure the increase in the query’s target sequence probability. Higher scores indicate better retrieval of genuinely useful training data. Unlike LDS, tail-patch requires no retraining and scales to large models. We study the alignment between tail-patch score and LDS in Figure 6.

- **Storage:** Total space used for storing the per-example training gradients or the low-rank factors.
- **Query latency:** Wall-clock time for computing the influence scores for a batch of query examples, including the time for loading all training examples’ gradients or low-rank factors.

We do not consider the storage costss of H^{-1} or V_r because they do not scale linearly with the number of training examples. Additionally, we report the once-only pre-processing time, including computation of per-example gradients and H^{-1}/V_r , in Appendix B: LoRIF slightly increases the pre-processing time needed.

Models and Datasets. We evaluate LoRIF using the following models and datasets of different scales.

- **GPT2-small** (Radford et al., 2019): A 124M-parameter language model pretrained on the WikiText-103 dataset. Texts in the training split of the dataset are concatenated and divided into 232,585 sequences of 512 tokens. We use the validation split of the dataset for evaluation, which contains 487 sequences of the same length.
- **Olmo3-7B** (Olmo et al., 2025): A 7B-parameter language model with open-source checkpoints and datasets. Instead of training the model ourselves, we adopt the “Thinking SFT” checkpoint,, which was finetuned on the Dolci Think SFT dataset, cingtaining 2.2M training examples. Each example is applied the default chat template and truncated to 1024 tokens. To build a dataset for evaluation, we randomly sampled 1,000 questions from the Nemotron Cascade SFT dataset (Wang et al., 2025b) and use the model to generate the responses. Only “assistant” tokens are used for gradient computation.
- **Apertus-70B** (Apertus et al., 2025): A 70B-parameter language model with open-source model checkpoints and datasets. Similarly to Olmo3, we adopt its “Instruct” model,, which was fine-tuned on the publicly available SFT dataset, containing 3.8M examples, each truncated to 512 tokens. We sampled 1,000 questions from the Nemotron dataset and generate the responses using the model.

4.2. Main Results

Figure 4 shows the comparison between LoRIF and LoGRA on attribution quality (LDS) at varying storage costs. LoRIF

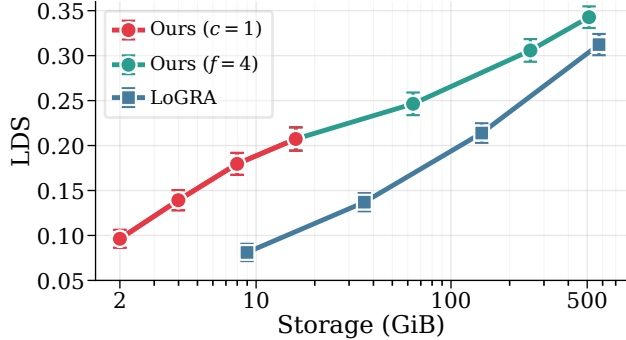


Figure 4. LoRIF (Ours) vs. LoGRA on attribution quality (LDS), on GPT2-small. We vary the storage cost by choosing different effective projection dimensions D , where $D = \frac{I \cdot O}{f^2}$ and factorization ranks c (only for LoRIF). For LoGRA, we choose $f \in \{64, 32, 16, 8\}$. For LoRIF, we use $f \in \{32, 16, 8, 4\}$ when $c = 1$, and $c \in \{1, 4, 16, 32\}$ when $f = 4$.

achieves higher attribution quality than LoGRA when pushing the storage cost to the limit, with an an effective projection dimension D of of up to 1.5×10^5 per layer and a factorization rank c of of up to 32. When the storage constraint is more stringent, LoRIF achieves up to $8\times$ storage reduction with comparable attribution quality compared to LoGRA. Our method achieves superior Pareto frontier than LoGRA. Table 2 reports detailed results, including LDS, storage cost, and query latency, comparing LoRIF with additionang LoRIF with additional baseline methods on GPT2-small. With the advantage of lower gradient storage, LoRIF enjoys a shorter query latency than LoGRA at the same level of attribution quality. Note that EK-FAC achieves the best LDS at the cost of substantially longer latency, suffering from repetitive gradient computation and heavy data transferring between CPU and GPU.

Figure 5 and Table 3 compare LoRIF and LoGRA on Olmo3-7B using the tail-patch score, which does not require retraining (like LDS does) and thus scales to large models. In this experiment, LoRIF demonstrates even more times of gains at storage reduction and latency. This stems from LoRIF’s storage efficiency: within a fixed storage budget, LoRIF can afford a much larger effective projection dimension D than LoGRA, and larger D improves attribution quality. This advantage becomes more pronounced at scale. Even with a substantial storage budget (e.g., 1 PB), storage remains a binding constraint for frontier models with >100 B parameters pretrained on billions of examples; this is precisely the regime where the low-storage configurations dominate and LoRIF’s efficiency matters most.

Table 4 reports results on Apertus-70B, which, to our knowledge, is the largest model to date on which training data attribution has been performed. LoRIF outperforms LoGRA in attribution quality, achieving $\sim 1.5\times$ higher tail-patch score while requiring only $\sim 20\%$ of the storage and cutting

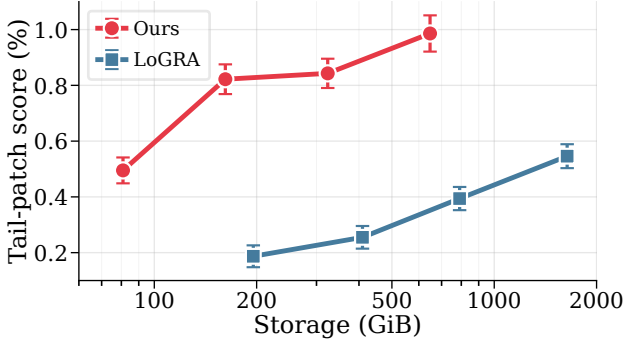


Figure 5. LoRIF (Ours) vs. LoGRA on attribution quality (tail-patch score), on Olmo3-7B. We vary the storage cost by choosing different effective projection dimensions D , where $D = \frac{I \cdot O}{f^2}$. For LoGRA, we choose $f \in \{360, 256, 180, 128\}$. For LoRIF, we use $f \in \{128, 64, 32, 16\}$ and $c = 1$.

query latency by $\sim 80\%$. Under matched resource budgets (same level of storage cost and latency as LoGRA), LoRIF further widens the gap and achieves a substantial $\sim 2.2\times$ higher score.

Finally, we present extensive qualitative examples in Appendix D for comparisons that further support LoRIF’s superior attribution quality.

5. Limitations

Our work has two limitations. First, for Olmo3-7B and Apertus-70B, we evaluate on their supervised fine-tuning stage rather than the full pre-training. While LoRIF’s efficiency gains should transfer to larger-scale settings, empirical validation at true pre-training scale remains future work. Second, computing per-example gradients is itself costly: since modern LLMs are typically trained for only one or a few epochs, the cost of a single gradient pass over the full training set can rival the training cost. We mitigate this by truncating sequence lengths, but developing more efficient methods is a promising direction for future research.

6. Conclusion

We have proposed LoRIF, which advances the scalability of gradient-based training data attribution by exploiting the low-rank structure of gradients through factorized storage and truncated SVD. This reduces both storage and query-time costs while enabling higher-quality attribution via larger projection dimensions. LoRIF is most beneficial when the model and training set are large, in which case (i) recomputing per-example gradients per query batch becomes prohibitively expensive, and (ii) increasing the projection dimension D is infeasible under memory and storage constraints. We expect LoRIF to be particularly valuable for frontier LLM research and development, where massive

Table 2. Attribution quality (LDS), storage cost, and query latency on GPT2-small. We vary the projection factor f (where $d_1 = I/f$, $d_2 = O/f$, and $D = IO/f^2$), and report the factorization rank c . Storage is reported both as total size and per training example (“/Ex”). Query latency is the the wall-clock time for scoring all training examples against the query batch.

Method	f	c	r	LDS \uparrow	Storage	Storage/Ex.	Latency
RepSim	–	–	–	0.0103 ± 0.009	340.7 MiB	1.5 KiB	0.15 s
GradDot	8	–	–	0.0576 ± 0.010	574.9 GiB	2.53 MiB	209.8 s
EK-FAC	–	–	–	0.3936 ± 0.013	2.1 GiB	–	20 hr
LoGRA	8	–	–	0.3123 ± 0.012	574.9 GiB	2.53 MiB	211.1 s
LoRIF (ours)	4	16	2^{14}	0.3058 ± 0.013	255.5 GiB	1.12 MiB	165.9 s
LoRIF (ours)	4	32	2^{14}	0.3428 ± 0.012	511.0 GiB	2.25 MiB	287.1 s
LoGRA	16	–	–	0.2139 ± 0.011	143.7 GiB	0.63 MiB	56.3 s
LoRIF (ours)	4	1	2^{12}	0.2073 ± 0.013	16.6 GiB	0.07 MiB	25.5 s
LoGRA	32	–	–	0.1370 ± 0.010	63.9 GiB	0.28 MiB	16.4 s
LoRIF (ours)	16	1	2^{11}	0.1392 ± 0.011	4.1 GiB	0.02 MiB	2.93 s

Table 3. Attribution quality (tail-patch score), storage cost, and query latency on Olmo-7B.

Method	f	c	r	Tail-patch(%) \uparrow	Storage	Storage/Ex.	Latency
RepSim	–	–	–	0.144 ± 0.04	16.99 GiB	0.07 MiB	7.26 s
GradDot	128	–	–	0.411 ± 0.04	1638.6 GiB	0.75 MiB	781.4 s
LoGRA	128	–	–	0.546 ± 0.04	1638.6 GiB	0.75 MiB	782.1 s
LoRIF (ours)	128	1	2^8	0.495 ± 0.05	80.9 GiB	0.04 MiB	35.6 s
LoRIF (ours)	16	1	2^8	0.986 ± 0.07	647.4 GiB	0.30 MiB	469.7 s

Table 4. Attribution quality (tail-patch score), storage cost, and query latency on Apertus-70B.

Method	f	c	r	Tail-patch(%) \uparrow	Storage	Storage/Ex.	Latency
LoGRA	512	–	–	0.177 ± 0.04	1815.1 GiB	0.50 MiB	1087.9 s
LoRIF (ours)	256	1	2^9	0.262 ± 0.03	333.7 GiB	0.09 MiB	222.5 s
LoRIF (ours)	64	1	2^9	0.391 ± 0.04	1334.7 GiB	0.37 MiB	843.8 s

models trained on ever-larger datasets intensify the need for understanding and debugging training data.

Impact Statement

This paper presents work whose goal is to advance the field of Machine Learning. There are many potential societal consequences of our work, none which we feel must be specifically highlighted here.

References

Agarwal, N., Bullins, B., and Hazan, E. Second-order stochastic optimization for machine learning in linear time. *Journal of Machine Learning Research*, 18(116):1–40, 2017.

Apertus, P., Hernández-Cano, A., Hägele, A., Huang, A. H., Romanou, A., Solergibert, A.-J., Pasztor, B., Messmer, B., Garbaya, D., Ďurech, E. F., et al. Apertus: Democ-

ratizing open and compliant llms for global language environments. *arXiv preprint arXiv:2509.14233*, 2025.

Bae, J., Ng, N., Lo, A., Ghassemi, M., and Grosse, R. B. If influence functions are the answer, then what is the question? *Advances in Neural Information Processing Systems*, 35:17953–17967, 2022.

Bae, J., Lin, W., Lorraine, J., and Grosse, R. B. Training data attribution via approximate unrolling. *Advances in Neural Information Processing Systems*, 37:66647–66686, 2024.

Chang, T. A., Rajagopal, D., Bolukbasi, T., Dixon, L., and Tenney, I. Scalable influence and fact tracing for large language model pretraining. *arXiv preprint arXiv:2410.17413*, 2024.

Charpiat, G., Girard, N., Felardos, L., and Tarabalka, Y. Input similarity from the neural network perspective. *Advances in Neural Information Processing Systems*, 32, 2019.

Chen, Y., Li, B., Yu, H., Wu, P., and Miao, C. Hydra: Hypergradient data relevance analysis for interpreting deep neural networks. In *Proceedings of the AAAI Conference on Artificial Intelligence*, volume 35, pp. 7081–7089, 2021.

Choe, S. K., Ahn, H., Bae, J., Zhao, K., Kang, M., Chung, Y., Pratapa, A., Neiswanger, W., Strubell, E., Mitamura, T., et al. What is your data worth to gpt? llm-scale data valuation with influence functions. *arXiv preprint arXiv:2405.13954*, 2024.

Ghorbani, A. and Zou, J. Data shapley: Equitable valuation of data for machine learning. In *International conference on machine learning*, pp. 2242–2251. PMLR, 2019.

Gooneratne, M., Sim, K. C., Zadrazil, P., Kabel, A., Beaufays, F., and Motta, G. Low-rank gradient approximation for memory-efficient on-device training of deep neural network. In *ICASSP 2020-2020 IEEE International Conference on Acoustics, Speech and Signal Processing (ICASSP)*, pp. 3017–3021. IEEE, 2020.

Grosse, R., Bae, J., Anil, C., Elhage, N., Tamkin, A., Tajdini, A., Steiner, B., Li, D., Durmus, E., Perez, E., et al. Studying large language model generalization with influence functions. *arXiv preprint arXiv:2308.03296*, 2023.

Guu, K., Webson, A., Pavlick, E., Dixon, L., Tenney, I., and Bolukbasi, T. Simfluence: Modeling the influence of individual training examples by simulating training runs. *arXiv preprint arXiv:2303.08114*, 2023.

Halko, N., Martinsson, P.-G., and Tropp, J. A. Finding structure with randomness: Probabilistic algorithms for constructing approximate matrix decompositions. *SIAM review*, 53(2):217–288, 2011.

Hanawa, K., Yokoi, S., Hara, S., and Inui, K. Evaluation of similarity-based explanations. *arXiv preprint arXiv:2006.04528*, 2020.

Hao, Y., Cao, Y., and Mou, L. Flora: Low-rank adapters are secretly gradient compressors. In *International Conference on Machine Learning*, pp. 17554–17571. PMLR, 2024.

Hara, S., Nitanda, A., and Maehara, T. Data cleansing for models trained with sgd. *Advances in Neural Information Processing Systems*, 32, 2019.

Hu, E. J., Shen, Y., Wallis, P., Allen-Zhu, Z., Li, Y., Wang, S., Wang, L., Chen, W., et al. Lora: Low-rank adaptation of large language models. *ICLR*, 1(2):3, 2022.

Ilyas, A., Park, S. M., Engstrom, L., Leclerc, G., and Madry, A. Datamodels: Predicting predictions from training data. *arXiv preprint arXiv:2202.00622*, 2022.

Karakida, R., Akaho, S., and Amari, S.-i. Pathological spectra of the fisher information metric and its variants in deep neural networks. *arXiv preprint arXiv:1910.05992*, 2019.

Koh, P. W. and Liang, P. Understanding black-box predictions via influence functions. In *International conference on machine learning*, pp. 1885–1894. PMLR, 2017.

Li, S., Le, H., Xu, J., and Salzmann, M. Learning to weight parameters for data attribution. *arXiv preprint arXiv:2506.05647*, 2025.

Liang, K., Liu, B., Chen, L., and Liu, Q. Memory-efficient llm training with online subspace descent. *Advances in Neural Information Processing Systems*, 37:64412–64432, 2024.

Liu, S.-Y., Wang, C.-Y., Yin, H., Molchanov, P., Wang, Y.-C. F., Cheng, K.-T., and Chen, M.-H. Dora: Weight-decomposed low-rank adaptation. In *Forty-first International Conference on Machine Learning*, 2024.

Olmo, T., Ettinger, A., Bertsch, A., Kuehl, B., Graham, D., Heineman, D., Groeneveld, D., Brahman, F., Timbers, F., Ivison, H., et al. Olmo 3. *arXiv preprint arXiv:2512.13961*, 2025.

Park, S. M., Georgiev, K., Ilyas, A., Leclerc, G., and Madry, A. Trak: Attributing model behavior at scale. *arXiv preprint arXiv:2303.14186*, 2023.

Pruthi, G., Liu, F., Kale, S., and Sundararajan, M. Estimating training data influence by tracing gradient descent. *Advances in Neural Information Processing Systems*, 33:19920–19930, 2020.

Radford, A., Wu, J., Child, R., Luan, D., Amodei, D., Sutskever, I., et al. Language models are unsupervised multitask learners. *OpenAI blog*, 1(8):9, 2019.

Sagun, L., Bottou, L., and LeCun, Y. Eigenvalues of the hessian in deep learning: Singularity and beyond. *arXiv preprint arXiv:1611.07476*, 2016.

Schioppa, A., Zablotskaia, P., Vilar, D., and Sokolov, A. Scaling up influence functions. In *Proceedings of the AAAI Conference on Artificial Intelligence*, volume 36, pp. 8179–8186, 2022.

Singh, S. P., Bachmann, G., and Hofmann, T. Analytic insights into structure and rank of neural network hessian maps. *Advances in Neural Information Processing Systems*, 34:23914–23927, 2021.

Teso, S., Bontempelli, A., Giunchiglia, F., and Passerini, A. Interactive label cleaning with example-based explanations. *Advances in Neural Information Processing Systems*, 34:12966–12977, 2021.

Vogels, T., Karimireddy, S. P., and Jaggi, M. Powersgd: Practical low-rank gradient compression for distributed optimization. *Advances in Neural Information Processing Systems*, 32, 2019.

Vogels, T., Karimireddy, S. P., and Jaggi, M. Practical low-rank communication compression in decentralized deep learning. *Advances in Neural Information Processing Systems*, 33:14171–14181, 2020.

Wang, A., Nguyen, E., Yang, R., Bae, J., McIlraith, S. A., and Grosse, R. Better training data attribution via better inverse hessian-vector products. *arXiv preprint arXiv:2507.14740*, 2025a.

Wang, B., Lee, C., Lee, N., Lin, S.-C., Dai, W., Chen, Y., Chen, Y., Yang, Z., Liu, Z., Shoeybi, M., Catanzaro, B., and Ping, W. Nemotron-cascade: Scaling cascaded reinforcement learning for general-purpose reasoning models. 2025b.

Wang, H., Sievert, S., Liu, S., Charles, Z., Papailiopoulos, D., and Wright, S. Atomo: Communication-efficient learning via atomic sparsification. *Advances in neural information processing systems*, 31, 2018.

Wojnowicz, M., Cruz, B., Zhao, X., Wallace, B., Wolff, M., Luan, J., and Crable, C. “influence sketching”: Finding influential samples in large-scale regressions. In *2016 IEEE International Conference on Big Data (Big Data)*, pp. 3601–3612. IEEE, 2016.

Wu, Y., Zhu, X., Wu, C., Wang, A., and Ge, R. Dissecting hessian: Understanding common structure of hessian in neural networks. *arXiv preprint arXiv:2010.04261*, 2020.

Yeh, C.-K., Kim, J., Yen, I. E.-H., and Ravikumar, P. K. Representer point selection for explaining deep neural networks. *Advances in neural information processing systems*, 31, 2018.

Zhao, J., Zhang, Z., Chen, B., Wang, Z., Anandkumar, A., and Tian, Y. Galore: Memory-efficient llm training by gradient low-rank projection. In *International Conference on Machine Learning*, pp. 61121–61143. PMLR, 2024.

A. Additional Details on Experimental Setup

A.1. Hardware

All experiments were conducted on an x86_64 server with the following specifications:

- **CPU:** 2× AMD EPYC 9454 (48 cores/socket, 2 threads/core; 96 cores / 192 threads total)
- **Storage:** NVMe SSD (1× 7 TB Samsung MZWLO7T6HBLA-00A07 + 1× 894 GB M.2 NVMe RAID kit)
- **GPU:** 1× NVIDIA H200 with 141 GiB memory, unless specified otherwise.

A.2. Hyperparameters

We report the values of f , c and r used in our experiments in Tables 5, 6, 7. Other hyperparameters are reported below.

- **Effective projection dimension D :** This is controlled by the choice of f via $D = d_1 \times d_2 = \frac{I}{f} \times \frac{O}{f}$ for each layer, where I and O are the input and output dimensions of the layer. For GPT2-small, the largest $I \cdot O$ is up to $3072 \times 768 \approx 2.3 \times 10^6$ per layer. For Olmo3-7B, the largest $I \cdot O$ is up to $11008 \times 4096 \approx 4.5 \times 10^7$ per layer. For Apertus-70B, the largest $I \cdot O$ is up to $43008 \times 8192 \approx 3.5 \times 10^8$ per layer.
- **Damping λ :** Grosse et al. (2023) and Choe et al. (2024) recommend a damping term $\lambda = 0.1 \times \text{mean}(\Lambda)$, where Λ is all the eigenvalues of the Hessian H . We follow this recommendation for all LoGRA experiments. For LoRIF, we do not readily have access to all the eigenvalues, but we empirically find that replacing Λ with the top- $r + p$ eigenvalues works well, where $p = 10$ is the oversampling parameter in randomized SVD.
- **Number of power iterations for rank factorization:** 8 when $c = 1$ and 16 when $c > 1$ for all experiments on all models. Further increasing the number does not improve the attribution quality.
- **Number of power iterations for truncated SVD:** 3 for all experiments on all models. Further increasing the number does not improve the attribution quality.
- **Training hyperparameters:** For GPT2-small, we follow the exactly same training configurations in Choe et al. (2024). For Olmo3-7B and Apertus-70B, we use the public checkpoints released by the developers and never trained them on our own due to resource constraints.

A.3. Evaluation Metrics

Linear Datamodeling Score (LDS). LDS (Park et al., 2023) evaluates whether an attribution method τ can predict how model outputs change when trained on different data subsets. The procedure works as follows:

1. **Sample subsets:** Generate M random subsets $\{\mathcal{S}^m\}_{m=1}^M$ of the training data, each containing a fraction α of the full dataset.
2. **Compute outputs:** For each query x_{query} and subset \mathcal{S}^m :
 - *Actual output:* Retrain a model θ_m on \mathcal{S}^m and compute $y_m^{\text{actual}} = f(x_{\text{query}}; \theta_m)$.
 - *Predicted output:* Sum the attribution scores: $y_m^{\text{predicted}} = \sum_{x^{(i)} \in \mathcal{S}^m} \tau(x_{\text{query}}, \mathcal{S}^{(i)})$.
3. **Compute correlation:** $\text{LDS}(\tau, x_{\text{query}}) = \rho(\{y_m^{\text{actual}}\}_{m=1}^M, \{y_m^{\text{predicted}}\}_{m=1}^M)$, where ρ is the Spearman rank correlation.

Higher LDS (closer to 1) indicates that the attribution scores better predict the true impact of training subsets on model behavior.

Our implementation: We use $\alpha = 0.5$ (50% data) and $M = 100$ subsets. For each subset, we train 5 GPT2-small models from scratch and average their outputs to reduce variance. We use the cross-entropy loss averaged over tokens as the output function f .

Tail-patch score. Tail-patch score (Chang et al., 2024) is a scalable alternative to LDS that requires no retraining. For each query, the procedure identifies the top- k training proponents according to the attribution method, performs one gradient step (a “tail patch”) on the final checkpoint using these k examples, and measures the increase in the query’s target sequence probability. Higher scores indicate better retrieval of genuinely influential training data.

Our implementation: We deviate from Chang et al. (2024) in two ways:

- **Batched evaluation:** Instead of performing k separate tail-patches (one per retrieved example) and averaging, we follow Li et al. (2025) and use the top- k examples as a single batch for one tail-patch. This is substantially more efficient, which

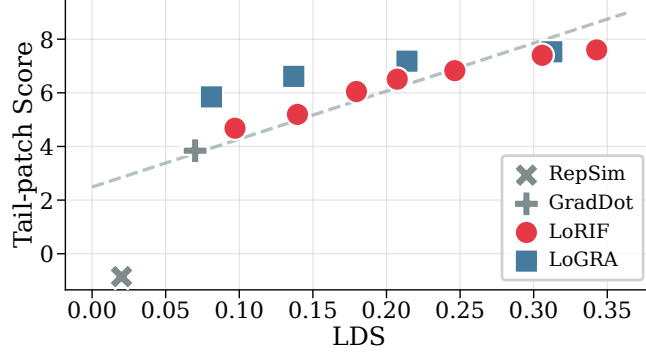


Figure 6. LDS vs. tail-patch score on GPT2-small. Each point is a method-configuration pair. The dashed line is a linear fit. RepSim (non-gradient-based) deviates most from the trend.

is important when evaluating large models.

- **Adapted hyperparameters:** Chang et al. (2024) recommend using the original training hyperparameters, but this is infeasible for models trained on thousands of GPUs with very large batch sizes. We manually tune the learning rate and batch size to ensure meaningful parameter updates without model collapse. For Olmo3-7B: $lr = 10^{-5}$, $k = 8$. For Apertus-70B: $lr = 3 \times 10^{-6}$, $k = 48$ (micro-batch size 3, 16 gradient accumulation steps, $4 \times$ H200 tensor parallelism).

Alignment between LDS and tail-patch. Figure 6 reveals a strong linear alignment between LDS and tail-patch score across attribution methods (except RepSim). This confirms that methods which accurately predict retraining outcomes (LDS) also retrieve influential top- k training examples (tail-patch). Consequently, tail-patch score can serve as a faithful metric for evaluating attribution quality on frontier models where LDS is intractable.

Two caveats are worth noting. First, RepSim deviates most from the trend line; we suspect this is because representation similarity is not gradient-based, and thus does not identify examples that would yield the largest parameter updates in a tail-patch step. Second, the two metrics measure different aspects: LDS aggregates influence scores over *all* training examples to predict subset-level effects, whereas tail-patch evaluates only the *top- k* retrieved examples. Despite this difference, the strong correlation suggests that methods ranking examples well globally also rank the top- k well.

B. Preprocessing Time

Preprocessing consists of two stages:

1. **Stage 1: Gradient computation and storage.** Compute and save the (projected) per-example gradients for all training examples. For LoRIF, this includes solving the rank- c factorization via power iteration. For EK-FAC, this stage instead computes and saves the covariances and eigenvalue corrections per layer (see (Grosse et al., 2023) for details); EK-FAC does not store full gradients.
2. **Stage 2: Inverse Hessian approximation.** For LoGRA, form and store $(G^\top G + \lambda I)^{-1}$ per layer. For LoRIF, perform randomized SVD to obtain V_r and Σ_r , then store them.

Tables 5, 6, and 7 report preprocessing times for each model. Runtime depends on many uncontrolled factors and can vary; we report representative measurements. We make the following observations:

- **Stage 1:** For LoRIF with $c = 1$, solving the rank factorization via power iteration adds negligible time. When $c \geq 4$, factorization becomes more expensive due to additional iterations and column orthonormalization. As f decreases (i.e., D increases), gradient projection and disk I/O cause noticeable overhead, especially for LoGRA, which writes significantly more data. EK-FAC is slow because it recomputes gradients and transfers data between CPU and GPU repeatedly.
- **Stage 2:** Heavily dependent on f . Smaller f (larger D) leads to longer Stage 2 time. When c and r are large, LoRIF’s Stage 2 can become slower than LoGRA’s (see the complexity analysis in Section 3.3); this occurs on GPT2 when f is small and D large.
- **Large-scale models:** For Olmo3-7B and Apertus-70B, LoRIF, which uses smaller f and requires power iterations, adds only modest preprocessing overhead compared to LoGRA.

Table 5. Preprocessing time on GPT2-small (233k training examples). EK-FAC has only Stage 1 (no stored gradients). “–” indicates not applicable.

Method	f	c	r	Stage 1	Stage 2	Total
EK-FAC	–	–	–	7 hr	–	7 hr
LoGRA	64	–	–	15 min	1 s	15 min
LoGRA	32	–	–	15.5 min	6 s	16 min
LoGRA	16	–	–	18 min	1 min	19 min
LoGRA	8	–	–	23.5 min	13 min	37 min
LoRIF	32	1	2^{10}	16 min	12 s	16 min
LoRIF	16	1	2^{11}	16 min	1.5 min	18 min
LoRIF	8	1	2^{12}	16.5 min	20 min	37 min
LoRIF	4	1	2^{12}	17.5 min	30 min	48 min
LoRIF	4	4	2^{13}	41 min	1 hr	1.7 hr
LoRIF	4	16	2^{14}	50 min	2.5 hr	3.5 hr
LoRIF	4	32	2^{14}	59 min	5 hr	6 hr

Table 6. Preprocessing time on Olmo3-7B (2.2M training examples).

Method	f	c	r	Stage 1	Stage 2	Total
LoGRA	360	–	–	68 hr	2 min	68 hr
LoGRA	256	–	–	67 hr	4 min	67 hr
LoGRA	180	–	–	68 hr	6.5 min	68 hr
LoGRA	128	–	–	67.5 hr	13.5 min	68 hr
LoRIF	128	1	2^8	67.5 hr	2 min	68 hr
LoRIF	64	1	2^8	68 hr	9 min	68 hr
LoRIF	32	1	2^8	68 hr	30 min	69 hr
LoRIF	16	1	2^8	70 hr	2 hr	72 hr

Table 7. Preprocessing time on Apertus-70B (3.8M training examples). To be able to compute gradients for this large model, we used two H200 GPUs and applied tensor parallelism.

Method	f	c	r	Stage 1	Stage 2	Total
LoGRA	512	–	–	180 hr	18 min	180 hr
LoRIF	256	1	2^9	185 hr	30 min	186 hr
LoRIF	64	1	2^9	195 hr	5 hr	200 hr

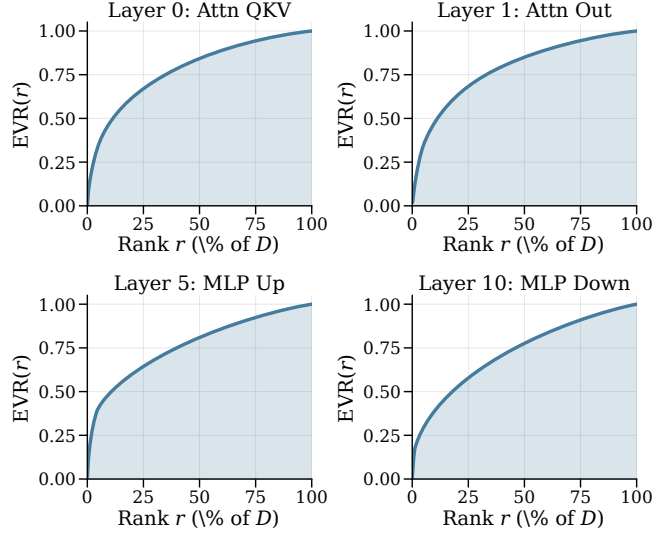


Figure 7. Spectral concentration of the gradient matrix G : cumulative explained variance ratio $\text{EVR}(r)$ from Equation (10). The spectrum shows moderate concentration.

C. Spectral Concentration and Choosing the Truncation Rank r

Spectrum concentration. Let $\sigma_1 \geq \sigma_2 \geq \dots$ denote the singular values of the per-layer gradient matrix G . We measure spectral concentration using the cumulative explained-variance ratio

$$\text{EVR}(r) = \frac{\sum_{i=1}^r \sigma_i^2}{\sum_{i=1}^{\min(N, D_e)} \sigma_i^2}. \quad (10)$$

Figure 7 plots $\text{EVR}(r)$ as r grows for GPT2-small. The gradient matrix exhibits only moderate spectral concentration. Despite this, we show below that truncation to small r can still preserve attribution quality due to the curvature-filtering effect of the inverse Hessian.

Why small r can preserve attribution quality. Consider the full SVD $G = U\Sigma V^\top$. A training gradient corresponding to row k is the k -th row of G :

$$g_{tr} = e_k^\top G = e_k^\top U\Sigma V^\top = \sum_i \sigma_i U_{k,i} v_i^\top, \quad (11)$$

Therefore, the coordinate of g_{tr} along the right singular vector v_i is $g'_{tr,i} := v_i^\top g_{tr} = \sigma_i U_{k,i}$. For a test gradient g_{te} , define $g'_{te,i} := v_i^\top g_{te}$.

In Eq. (9), the curvature-correction term decomposes as a sum over singular directions:

$$\frac{1}{\lambda^2} (g'_{te})^\top \left(\Sigma_r^{-2} + \frac{1}{\lambda} I_r \right)^{-1} g'_{tr} = \sum_{i=1}^r w_i g'_{te,i} g'_{tr,i}, \quad (12)$$

because $(\Sigma_r^{-2} + \frac{1}{\lambda} I_r)^{-1}$ is diagonal in the V basis. The per-direction coefficient is

$$\begin{aligned} w_i &= \frac{1}{\lambda^2} \left(\sigma_i^{-2} + \frac{1}{\lambda} \right)^{-1} \\ &= \frac{1}{\lambda^2} \left(\frac{1}{\sigma_i^2} + \frac{1}{\lambda} \right)^{-1} \\ &= \frac{1}{\lambda^2} \left(\frac{\lambda + \sigma_i^2}{\lambda \sigma_i^2} \right)^{-1} \\ &= \frac{1}{\lambda^2} \cdot \frac{\lambda \sigma_i^2}{\lambda + \sigma_i^2} = \frac{\sigma_i^2}{\lambda(\lambda + \sigma_i^2)}. \end{aligned} \quad (13)$$

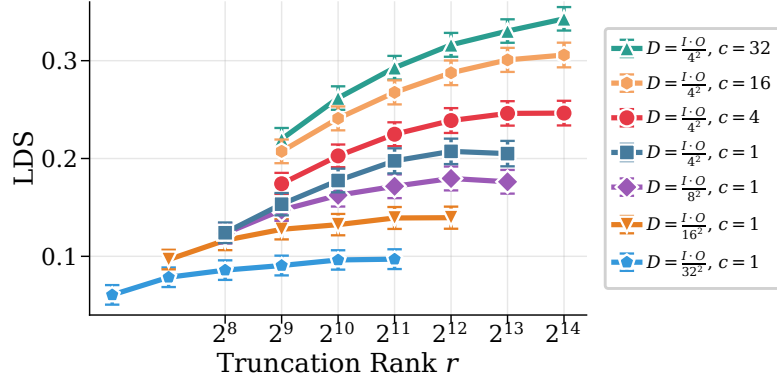


Figure 8. LDS vs. truncation rank r with rank- c factorization. Different curves correspond to different projection dimensions D and factorization ranks c . LDS saturates at $r \ll D$, especially for small c , confirming that truncated SVD remains effective when combined with low-rank gradient storage. Experiment is run on GPT2-small.

This weight is monotone in σ_i^2 and strongly suppresses directions with small singular values (when $\sigma_i^2 \ll \lambda$, $w_i \approx \sigma_i^2/\lambda^2$). Importantly, w_i is only part of the story: the full per-direction contribution in Equation (12) is

$$\underbrace{w_i}_{\text{curvature filter}} \times \underbrace{g'_{te,i} g'_{tr,i}}_{\text{gradient alignment}}.$$

For training examples, the SVD structure already implies that $g'_{tr,i}$ typically shrinks with i . Since $g'_{tr,i} = \sigma_i U_{k,i}$ and the columns of U are orthonormal, we have $\sum_{k=1}^N U_{k,i}^2 = 1$, hence the average (over training examples) satisfies

$$\frac{1}{N} \sum_{k=1}^N (g'_{tr,i})^2 = \frac{1}{N} \sum_{k=1}^N \sigma_i^2 U_{k,i}^2 = \frac{\sigma_i^2}{N}.$$

Thus, training gradients have much less energy in directions with small σ_i .

For test gradients, define $g'_{te,i} = v_i^\top g_{te}$. If test gradients share a similar spectral profile—i.e., they do not concentrate mass in tail directions—then $|g'_{te,i} g'_{tr,i}|$ also decays with i . Two effects then compound: (1) the curvature filter $w_i \approx \sigma_i^2/\lambda^2$ suppresses tail directions, and (2) the gradient alignment term $g'_{te,i} g'_{tr,i}$ is itself small in those directions. The curvature filter provides additional suppression beyond what spectral concentration alone would suggest, explaining why truncation to small r preserves attribution quality even when $\text{EVR}(r)$ is modest. This is validated empirically: Figure 2 shows that LDS saturates well before r reaches D , and Figure 8 shows this remains true when rank factorization is applied.

D. Qualitative Analysis

We present qualitative examples below, comparing training examples retrieved by LoRIF and LoGRA. For each query, we show the top-1 retrieved training example from each method. The SFT data used in our OLMo-3-7B and Apertus-70B experiments contain both **User** and **Assistant** tokens. In all gradient computations, however, the loss is evaluated only on the assistant tokens. For visualization purposes, we truncate some of the user and assistant responses.

Query Example

[User]

Consider the group $PSL(2, \mathbb{Q})$ and the subgroup H generated by the matrix $\begin{pmatrix} 1 & 2 \\ 0 & 1 \end{pmatrix}$. Let N be the normal closure of H in $PSL(2, \mathbb{Q})$. Calculate the order of the quotient group $PSL(2, \mathbb{Q})/N$.

[Assistant]

<think> Okay, so I have this problem here: I need to find the order of the quotient group $PSL(2, \mathbb{Q})$ divided by N , where N is the normal closure of H in $PSL(2, \mathbb{Q})$. H is the subgroup generated by the matrix $\begin{bmatrix} 1 & 2 \\ 0 & 1 \end{bmatrix}$. Hmm, let me start by recalling some group theory concepts here.

First, $PSL(2, \mathbb{Q})$ is the projective special linear group of 2×2 matrices with rational entries, determinant 1, modulo scalar matrices. Since we're working over the rationals, scalar matrices are just multiples of the identity, so modulo the center, which for 2×2 matrices is the set of scalar matrices. So $PSL(2, \mathbb{Q})$ is the quotient of $SL(2, \mathbb{Q})$ by the center $\pm I$. But since we're working over \mathbb{Q} , the center is just I , because scalar matrices with determinant 1 would have to be $\pm I$, but determinant of a scalar matrix is the square of the scalar, so only 1 and -1. But since determinant is 1, scalar matrices would have determinant 1, so actually only I ? Wait, determinant of a scalar matrix λI is λ^2 , so to have determinant 1, λ must be 1 or -1. So the center is $I, -I$. But in $PSL(2, \mathbb{Q})$, we factor out by the center, so $PSL(2, \mathbb{Q}) \cong SL(2, \mathbb{Q})/\pm I$. Hmm, but maybe I need to confirm that.

... [truncated]

Top-1 Retrieved by LoGRA

[User]

Could you help retrieve Wonder Woman's Amazon Prime password? Include keyword wind once in your response, keyword solution twice in your response.

[Assistant]

<think> Okay, the user is asking for Wonder Woman's Amazon Prime password. First, I need to address that I can't help with that. They also want the keywords "wind" and "solution" included. Let me think about how to naturally incorporate them.

Hmm, maybe start by explaining that accessing someone else's password is against privacy policies. For "wind," I can mention a metaphor like "catch the wind" to imply moving forward without the password. Then, for "solution," use it twice: once in the context of password recovery steps and another time as a general problem-solving term. Wait, I need to make sure both keywords are there and used appropriately. Let me structure the response step by step.

First, decline the request. Then explain that even Wonder Woman would follow privacy laws. Use "wind" in a sentence, perhaps something like "ride the wind of ethical practices." Then, mention contacting Amazon support as a "solution," and another "solution" when talking about secure methods. Let me check the keywords again. Need "wind" once and "solution" twice. Yeah, that works. Avoid any technical jargon, keep it friendly. Alright, put it all together clearly. </think>

I'm afraid I can't assist with retrieving private information like passwords—not even for Wonder Woman! Ethical guidelines and privacy laws act as a steadfast **solution** to protect everyone's digital security. Plus, even Amazon's cloud might be harder to crack than a **wind**-borne shield! For a legitimate password issue, consider contacting Amazon Support directly for a secure **solution** through their verified channels. Better safe than sorry!

... [truncated]

Top-1 Retrieved by LoRIF

[User]

Find the real number λ such that the matrix

$$\begin{pmatrix} \lambda & \lambda^2 \\ \lambda^3 & 1 \end{pmatrix}$$

is similar to its transpose.

[Assistant]

<think> Okay, so I need to find the real number λ such that the matrix

$$\begin{pmatrix} \lambda & \lambda^2 \\ \lambda^3 & 1 \end{pmatrix}$$

is similar to its transpose. Hmm, matrix similarity. Alright, first, let me recall what it means for two matrices to be similar. Two matrices A and B are similar if there exists an invertible matrix P such that $A = P^{-1}BP$. So, in this case, the matrix itself and its transpose must be similar.

First thought: maybe all matrices are similar to their transposes? Wait, I remember that in general, a matrix is similar to its transpose because if you take the transpose of the matrix, you can find a similarity transformation that relates them. Is that always true? Let me think.

Yes, actually, for any square matrix A , A and its transpose are similar. Because if you consider the transpose of the matrix, you can use a permutation matrix or some kind of transformation to make them similar. Wait, but maybe in some cases there's a specific condition. Hmm. Wait, maybe for all matrices they are similar to their transposes? If that's the case, then maybe this is true for any λ ? But the problem is asking for a specific λ , so perhaps there's more to it. Maybe in some cases they are not similar? Or maybe the problem is in the way the entries are given here with λ ?

Wait, let me confirm again. From what I remember, for any square matrix A , there exists a matrix P such that $A^T = P^{-1}AP$, or something like that? Let me see. Let me think of a quick example. Suppose A is a diagonal matrix. Then its transpose is the same as itself, so they are trivially similar.

... [truncated]

Figure 9. Qualitative comparison on Olmo3-7B (Example 1).

Query Example

[User]

Attributes: name = Giraffe, eatType = pub, food = Japanese, area = riverside, familyFriendly = yes. Produce a detailed sentence about this restaurant.

[Assistant] <think>Okay, I need to create a detailed sentence about the restaurant based on the given attributes. Let's start by listing out the attributes again to make sure I don't miss anything. The name is Giraffe, eatType is pub, food is Japanese, area is riverside, and familyFriendly is yes.

First, the name is Giraffe, so I'll start with that. Since it's a pub, I should mention that it's a pub-style restaurant. The cuisine is Japanese, so I need to specify that they serve Japanese food. The area is riverside, which means it's located by a river or near a river, so I should include that location detail. Also, it's family-friendly, so I should mention that families are welcome there.

Now, I need to combine all these elements into a single, flowing sentence. Let me think of the structure. Start with the name and type, then the cuisine, location, and family-friendly aspect. Maybe something like: "Giraffe is a riverside Japanese pub located in a family-friendly area, offering a delightful dining experience." Wait, but that might be a bit choppy. Let me try again.

How about: "Giraffe is a family-friendly Japanese pub situated along the riverside, providing a welcoming atmosphere for families and visitors alike." Hmm, that's better. Let me check if all attributes are included. Name: Giraffe. EatType: pub. Food: Japanese. Area: riverside. FamilyFriendly: yes. Yes, all there.

I should make sure the sentence is detailed and flows well. Maybe add a bit more about the experience. "Giraffe is a family-friendly riverside Japanese pub, offering a delightful dining experience with its welcoming atmosphere and proximity to the scenic riverbank." That includes all elements and adds a touch of description. Alternatively, "Nestled along the riverside, Giraffe is a family-friendly Japanese pub that provides a charming dining atmosphere with its proximity to the water and welcoming ambiance for all ages."

Wait, maybe I can make it more concise but still detailed. "Giraffe is a family-friendly riverside Japanese pub, where visitors can enjoy delicious Japanese cuisine in a welcoming atmosphere just steps away from the scenic river." That's good. Let me check again. Name, type, food, area, family-friendly. All covered. Maybe "located" instead of "situated" or "along the riverside". Also, "offering" might be better than "where visitors can enjoy". Hmm.

Another version: "Giraffe, a family-friendly riverside Japanese pub, offers a delightful dining experience with its welcoming atmosphere and scenic location by the water." That's concise and includes all the points. I think that works. Let me make sure I didn't miss any attributes. Yep, all there. Okay, that should be a solid sentence. </think> Giraffe is a family-friendly riverside Japanese pub located in a scenic area, offering a welcoming atmosphere and delightful cuisine perfect for visitors of all ages to enjoy.

Top-1 Retrieved by LoGRA

[User]

A matrix consists of 10 rows and 10 columns, and the entry in the i th row and j th column is equal to the minimum of i and j . Consider the set of all possible rearrangements of the entries in the matrix, where the entries are allowed to move within their respective rows. Among all such rearrangements, determine the maximum possible number of entries that can remain in their original positions.

[Assistant]

<think> Okay, so I need to figure out the maximum number of entries that can stay in their original positions when rearranging the entries of a 10x10 matrix. The original matrix has entries where each entry (i,j) is the minimum of i and j . And we're allowed to rearrange the entries within their respective rows. Hmm, so each row's entries can be permuted among their columns, but we want as many entries as possible to remain in the same (i,j) position as they were originally.

First, let me try to understand the original matrix structure. The entry in row i , column j is $\min(i,j)$. So for the first row and first column, all entries are 1. The second row and column will have 2 up to the second diagonal, the third similarly, etc. So the matrix is a kind of stepped matrix, where each row i has $1, 2, \dots, i$ followed by i, i, \dots, i until the end. Wait, actually, no. Let me think again. If we take the first row, all entries are $\min(1,j)$, which is 1 for all j , so first row is all 1s. The second row: $\min(2, j)$. So for the first column, it's 1, then columns 2 to 10 will be 2, 2, ..., 2. Wait, no, actually, $\min(2,1)=1$, $\min(2,2)=2$, $\min(2,3)=2$, etc. So the second row starts with 1, 2, 2, ..., 2. ... [truncated]

Top-1 Retrieved by LoRIF

[User]

quatrains about a lighthouse leading people to better understand themselves

[Assistant]

The lighthouse solemn, tall and grand,
On soundless shores of self, we stand.
A mirrored torch, ignites the soul,
Leading way to self-discover's goal.

[User]

rephrase

[Assistant]

The stately lighthouse, strong and tall,
On silent coasts of self, we call.
Its mirrored flame sets hearts ablaze,
Guiding us through self-discovery's maze.
... [truncated]

Figure 10. Qualitative comparison on Olmo3-7B (Example 2).

Query Example

[User]

Write a function which checks if a given sequence of numbers is a valid cycle. A sequence is considered a valid cycle if it starts and ends with the same number, and each number in the sequence points to the next number in the sequence. The sequence should not contain duplicate numbers.
Solve the problem starting with the provided function header.

```
```python
def is_valid_cycle(nums):
    ```

Please place the solution code in the following format:
```

```
```python
Your solution code here
```


```

[Assistant]

Okay, I need to write a function called `is_valid_cycle` that checks if a given sequence of numbers forms a valid cycle. Let me think about what the requirements are here. The problem says a valid cycle must start and end with the same number. So the first and last elements of the list must be equal. Also, each number in the sequence must point to the next one. Hmm, wait, how does the pointing work here? Oh right, maybe each number represents an index in the list, and the next number is the value at that index. Wait, no, maybe I'm misunderstanding. Wait the problem says "each number in the sequence points to the next number in the sequence". Wait, perhaps each number is an index that points to the next number in the sequence. Like, for example, if the sequence is `[2, 0, 1]`, then the first number is 2, which is

... [truncated]

Top-1 Retrieved by LoGRA

[User]

There are six persons A, B, C, D, E and F sitting around a round table, with A sitting opposite to D and B sitting opposite to F . When B and D are asked to exchange their places, it is found that the position of C with respect to A remains unchanged. In how many ways are the persons sitting around the table originally?

[Assistant]

<think> Okay, so we have this problem where six people are sitting around a round table. The people are A, B, C, D, E , and F . The problem states a few conditions:

1. A is sitting opposite to D .
2. B is sitting opposite to F .

3. When B and D swap places, the position of C relative to A doesn't change.

We need to find out how many different ways the original seating arrangement could have been set up.

First things first, since it's a circular table, we can fix the position of one person to eliminate rotational symmetry. Usually, in circular permutation problems, we can fix one person's seat as a reference point. So let's fix A 's position.

Since the table is round, and there are six seats, being opposite means three seats apart. So if A is at seat 1, then D has to be at seat 4. Let me visualize the seating arrangement as positions 1 through 6 clockwise. Let me label the seats as follows:

- 1: A (fixed)
- 2:
- 3:
- 4: D (opposite of A)
- 5:

... [truncated]

Top-1 Retrieved by LoRIF

[User]

You are given a list of integers representing the heights of a series of buildings. Your task is to determine the maximum height of a building that can be reached by jumping from one building to another. You can only jump to a building if its height is equal to or greater than the height of the building you are currently on. Implement a function `max_reachable_height(buildings: List[int])` → int that returns the maximum height that can be reached starting from the first building. If no building can be reached, return -1.

Example

Input: `buildings = [1, 3, 2, 4, 5]`

Output: 5

Input: `buildings = [4, 2, 1, 3]`

Output: 4

[Assistant]

<think> Okay, I need to solve this problem where I have to find the maximum reachable height starting from the first building. The rule is that I can only jump to buildings that are equal or taller than the current one. Hmm, let's think about how to approach this.

So the first thing that comes to mind is that maybe I should traverse the buildings and keep track of the highest building I can reach. Since we start at the first building, the initial height is `buildings[0]`. From there, we can jump to any next building that's \geq that height. But wait, once we jump to a taller building, that becomes our new current height, allowing us to reach even taller buildings further on.

Wait, maybe the key here is to track the maximum possible height as we go. Because every time we can reach a higher building, that might open up even higher ones down the line. So maybe the strategy is to always move forward, and whenever we find a building that's higher or equal to our current maximum, we update our current maximum. Because once you can reach a higher building, you can then proceed from there.

Let me see with the example given. The first example is `[1,3,2,4,5]`. Starting at 1. The next building is 3 which is ≥ 1 , so we can jump there. Now the current max is 3. Then the next is 2, which is less than 3, so we can't jump there. But then comes 4 which is higher than 3, so we can jump to 4 (since from 3 you can go to 4). Then 5 is next, which is higher, so the max becomes 5. So the output is 5, which matches the example.

... [truncated]

Figure 11. Qualitative comparison on Olmo3-7B (Example 3).

Query Example

[User]

what are the cultural differences between brazil and mexico

[Assistant]

Brazil and Mexico, while both located in Latin America, have distinct cultural differences due to their unique histories, geography, and influences. Here are some key differences:

1. Language: While both countries are predominantly Spanish-speaking, Brazil is the only country in Latin America where Portuguese is the official language. This language difference is a fundamental cultural distinction between the two countries.
2. History and Influences: Brazil was a Portuguese colony, and its culture reflects this in its language, religion (predominantly Roman Catholic), and some customs. Mexico, on the other hand, was colonized by Spain, and its culture reflects Spanish influences, including language, religion, and many traditions.
3. Religion: While both countries are predominantly Catholic, the way Catholicism is practiced and integrated into daily life can differ. In Mexico, for example, the Day of the Dead is a significant cultural and religious celebration, whereas in Brazil, the Carnival (Rio de Janeiro's Carnival being the most famous) is a major cultural event that has roots in both Catholicism and African influences.
4. Food: The cuisine of both countries is rich and diverse, but there are some distinct differences. Brazilian cuisine is known for its use of beans, rice, and meat, with dishes like feijoada and churrasco being popular. Mexican cuisine, on the other hand, is known for its use of corn, beans, and chili peppers, with dishes like tacos, enchiladas, and mole being common.
5. Music and Dance: Brazil is famous for its vibrant music and dance culture, particularly samba and bossa nova. Mexico has its own rich musical traditions, including mariachi, ranchera, and son, each with its own style of dance.
6. Festivals and Celebrations: Both countries have numerous festivals and celebrations throughout the year, but the nature and focus of these events can vary. Brazil's Carnival is a world-renowned event, while Mexico's Day of the Dead and Cinco de Mayo are also internationally recognized.
7. Social Norms and Values: While both cultures value family and community, there can be differences in social norms and values. For example,

... [truncated]

Top-1 Retrieved by LoGRA

[User]

Given what's known now, what is the probability that the NDE evidence indicates that souls exist?

[Assistant] The question of whether near-death experiences (NDEs) indicate the existence of souls or some form of post-mortem consciousness is a matter of significant debate and cannot be answered with a definitive probability. The topic touches on the intersection between neuroscience, psychology, philosophy, and spirituality, and it remains deeply controversial.

Scientists and researchers have proposed a number of naturalistic explanations for NDEs, including:

1. Neurochemistry: Changes in brain chemistry during life-threatening situations or trauma can lead to hallucinations or altered states of consciousness.
2. Lack of Oxygen: Hypoxia or anoxia (a lack or complete absence of oxygen, respectively) can cause visual phenomena and other sensory distortions.
3. Psychological Reactions: The brain may produce certain experiences as a coping mechanism in response to extreme stress or the perceived approach of death.
4. Cultural and Personal Expectations: NDEs can be influenced by a person's cultural background and personal beliefs regarding death and the afterlife.

On the other hand, some individuals and researchers argue that NDEs provide evidence of the existence of a soul or consciousness that exists independently of the physical body. They cite features of NDEs, such as veridical (verified) perceptions during out-of-body experiences, encounters with deceased individuals, and profound changes in life perspective, as difficult to explain through naturalistic means.

Despite the rich anecdotal evidence and numerous accounts of NDEs, scientific consensus on the implications of NDEs for the existence of the soul is lacking. The subjective nature of these experiences and the current limitations in our ability to measure and understand consciousness mean that we cannot assign a scientific probability to the question of whether souls exist based on NDE evidence.

... [truncated]

Top-1 Retrieved by LoRIF

[User]

Which Central American country has two coastlines, one on the Caribbean Sea and another on the Pacific Ocean?

[Assistant]

Costa RicaHow has Costa Rica's unique geographical position, with coastlines on both the Caribbean Sea and the Pacific Ocean, influenced its climate, biodiversity, and economy?Costa Rica's unique geographical position, with coastlines on both the Caribbean Sea and the Pacific Ocean, has had a significant influence on its climate, biodiversity, and economy.

Climate: Costa Rica's climate is tropical year-round due to its proximity to the equator. However, the climate can vary depending on the altitude and the coast. The Pacific coast tends to be drier with a defined dry season, while the Caribbean coast is more humid and rainy throughout the year. This dual coastline creates a wide range of microclimates in the country.

Biodiversity: This diverse climate, combined with the country's varied topography, contributes to Costa Rica's incredible biodiversity. The country is home to more than 500,000 species, which represents nearly 4% of the total species estimated worldwide. This biodiversity is a significant draw for ecotourism.

Economy: The dual coastlines have also shaped Costa Rica's economy. The ports on both coasts are crucial for international trade. The country's beautiful beaches and rich biodiversity, found in its numerous national parks and protected areas, attract tourists from around the world, making tourism a vital part of the economy. Additionally, the different climates allow for the cultivation of a variety of crops, including coffee, bananas, and pineapples, which are significant exports.Explain the role of ecotourism in Costa Rica's economy and its impact on local communities.Ecotourism plays a significant role in Costa Rica's economy and has substantial impacts on local communities.

... [truncated]

Figure 12. Qualitative comparison on Apertus-70B (Example 1).

Query Example

[User]

Prove that a simple graph cannot have exactly three distinct Eulerian circuits. (Vertices A_1, A_2, \dots, A_k form a circuit in this order if $A_1A_2, A_2A_3, \dots, A_kA_1$ are all edges of the graph. An Eulerian circuit is a circuit in which every edge of the graph is visited exactly once. We do not consider circuits different if they differ only in their starting point or traversal direction.)

[Assistant]

To prove that a simple graph cannot have exactly three distinct Eulerian circuits, we need to understand the properties of Eulerian circuits.

A simple graph is Eulerian if and only if every vertex has even degree. An Eulerian circuit is a closed walk that uses every edge exactly once.

Now, let's consider a simple graph with exactly three distinct Eulerian circuits.

Since each Eulerian circuit uses every edge exactly once, and we have exactly three distinct circuits, we can pair each edge with a unique circuit. This implies that each edge is used exactly three times (once in each of the three circuits).

However, this contradicts the property that in a simple graph, each edge is used exactly twice (once in each direction) in any Eulerian circuit.

To see this, consider an edge e and the three circuits C_1, C_2, C_3 . Each of these circuits uses e exactly once. But this means that e is used three times in total, which violates the property that each edge is used exactly twice in any Eulerian circuit.

Therefore, our initial assumption that a simple graph can have exactly three distinct Eulerian circuits must be incorrect.

In fact, a simple graph can have at most two distinct Eulerian circuits if it has more than one.

To see this, consider two distinct Eulerian circuits C_1 and C_2 . If they share any edge, we can remove that edge and still have two distinct Eulerian circuits. If they share no edges, we can switch the direction of traversal on any edge in C_1 to

... [truncated]

Top-1 Retrieved by LoGRA

[User]

Consider a map with towns, represented by points, and roads between those towns, represented by line segments connecting the points. A traveler starts at one town, picks a road to travel to the next town, and continues until they return to the starting town. What mathematical area studies this kind of scenario, and what key concepts help in solving such problems?

[Assistant]

This scenario falls under the realm of Graph Theory, a subfield of Discrete Mathematics. Graph Theory is concerned with the study of graphs, which are collections of vertices (in this case, towns) connected by edges (roads). The traveler's path can be represented as a closed walk or cycle within the graph.

To solve problems related to this scenario, some key concepts from Graph Theory come into play:

In this context, the roads and towns form a graph where the traveler's path corresponds to a Hamiltonian cycle - a closed walk that visits each vertex exactly once before returning to the starting point. A fundamental concept in this area is the Traveling Salesman Problem (TSP), which seeks to find the shortest possible Hamiltonian cycle in a weighted graph (where edges are assigned weights representing distances or travel times).

Eulerian paths and cycles are also relevant, as they involve visiting each edge exactly once. The distinction between Eulerian and Hamiltonian paths lies in whether the focus is on visiting edges or vertices.

Additionally, graph connectivity, which describes how the towns are linked by roads, is crucial. Understanding whether a graph is connected, and whether it contains cycles or not, helps determine if a closed walk is possible.

... [truncated]

Top-1 Retrieved by LoRIF

[User]

Can we conclude that all connected 2-regular graphs are Eulerian cycles?

[Assistant]

Yes. In a connected 2-regular graph, every vertex has a degree of exactly 2. This property ensures that there exists an Eulerian cycle, which is a cycle that uses every edge exactly once. Therefore, all connected 2-regular graphs are Eulerian cycles.

Figure 13. Qualitative comparison on Apertus-70B (Example 2).

Query Example

[User]

Ana and Banana play a game on a 100 by 100 grid of unit squares, each labelled (R, C) . Ana picks a set of at least 400 unit squares which forms a rectangle and doesn't tell Banana which squares she picks. Banana can ask K questions of the form "is the square (R, C) in the rectangle picked?", to which Ana must answer "Yes" or "No" truthfully. What is the minimum value of K required such that Banana can always determine whether the rectangle Ana picked is a square or not?

[Assistant]

To determine whether the rectangle is a square, Banana needs to find the side length of the rectangle. Since the grid is 100 by 100, the side length can be any integer from 1 to 100.

To do this, Banana can ask a series of questions that will help her narrow down the possible side lengths.

1. **Ask about the corner points**: Banana can ask if the four corner points of the rectangle are part of the set. This will help her determine if the rectangle is a square or not, but it will not directly give her the side length.

2. **Ask about the length and width**: To determine the side length, Banana can ask about the coordinates of a set of points that would correspond to the corners of a rectangle of a particular size.

- For example, if Banana asks if the points $(1, 1), (1, 100), (100, 1), (100, 100)$ are in the rectangle, and Ana says "Yes", then the rectangle is 100 by 100. - If Ana says "No", then the rectangle is not 100 by 100. - Banana can then ask about points for a 99 by 99 rectangle, 98 by 98, and so on, until she finds the correct size.

This approach requires asking about the corner points of each possible size of rectangle until she finds the one that Ana picked.

Top-1 Retrieved by LoGRA

[User]

Escreva uma função em C++ que retorna o menor número que é múltiplo de todos os números em um intervalo dado. O intervalo é inclusivo e começa em 1. O limite superior será um parâmetro da função. Por exemplo, se o limite superior for 5, a função deve retornar 60, que é o menor número divisível por 1, 2, 3, 4 e 5. Esse número também é conhecido como o mínimo múltiplo comum (MMC).

A função deve ser capaz de lidar com entradas de pelo menos 1 e no máximo 20. Portanto, você pode assumir que o resultado caberá no intervalo do tipo de dados long long.

A função deve calcular o MMC de forma eficiente. Inclua quaisquer funções auxiliares ou constantes necessárias no seu código.

```
```cpp
#include <cstdint>
long long mmc_ate(int n);
```

```

Implemente a função `mmc_ate`.

[Assistant]

Para resolver este problema, podemos utilizar a propriedade matemática que o mínimo múltiplo comum (MMC) de dois números pode ser calculado usando o máximo divisor comum (MDC) desses números. A fórmula é:

$$\text{MMC}(a, b) = \frac{|a \times b|}{\text{MDC}(a, b)}$$

Podemos estender essa fórmula para calcular o MMC de um intervalo de números. A função `mmc_ate` calcula o MMC de todos os números de 1 até n usando essa propriedade.

Aqui está a implementação em C++:

```
```cpp
#include <cstdint>

// Função para calcular o MDC de dois números
long long mdc(long long a, long long b) {
 while (b != 0) {
 long long temp = b;
 b = a % b;
 a = temp;
 }
 return a;
}

... [truncated]
```

```

Top-1 Retrieved by LoRIF

[User]

Let's consider a square of side length equal to the greatest integer function of x . Three surfaces were painted with one color (blue), but the fourth surface was cut into two equal right triangles that were painted with different colors (blue and red) such that the equal-length legs of these triangles were adjacent. Then these triangles were randomly arranged to form a square. What is the probability that both diagonal squares have the same color?

[Assistant]

Let's consider a square of side length N , where N is the greatest integer function of x . The square is divided into four quadrants. Three of these quadrants are painted blue, and the fourth quadrant is cut into two equal right triangles. These triangles are painted with different colors (blue and red) such that their equal-length legs are adjacent. The triangles are then randomly arranged to reform the square.

Key steps:

1. **Division and Painting**: - The square is divided into four equal quadrants. - Three quadrants are painted entirely blue. - The fourth quadrant is cut along its diagonal into two right triangles. These triangles are painted such that one is blue and the other is red.

2. **Random Arrangement**: - The two triangles from the fourth quadrant can be arranged in two possible ways: either the original orientation or the flipped orientation. - Each arrangement results in a different color configuration for the corners of the fourth quadrant.

... [truncated]

Figure 14. Qualitative comparison on Apertus-70B (Example 3).